Title
STATISTICAL EMISSION OF LARGE FRAGMENTS: A GENERAL THEORETICAL APPROACH

Author
Moretto, Luciano G.

Publication Date
1975

Submitted to Nuclear Physics A

LBL-3454
Preprint c.2

STATISTICAL EMISSION OF LARGE FRAGMENTS: A GENERAL THEORETICAL APPROACH

Luciano G. Moretto

January 1975

Prepared for the U. S. Atomic Energy Commission
under Contract W-7405-ENG-48

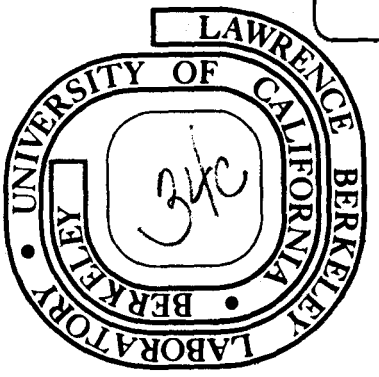

DISCLAIMER

STATISTICAL EMISSION OF LARGE FRAGMENTS: A GENERAL THEORETICAL APPROACH*

Luciano G. Moretto†

Department of Chemistry and
Lawrence Berkeley Laboratory
University of California
Berkeley, California 94720

ABSTRACT: A theory for the statistical emission of large fragments is developed. In analogy with the fission saddle point, a ridge line in the potential energy surface is defined which controls the decay width of the system into any two given fragments. The normal modes at the ridge are separated into three classes: decay modes, amplifying modes, and non-amplifying modes. Amplifying modes are those whose thermal fluctuations are amplified and lead to a broadening of the kinetic energy distribution. Analytical expressions for the kinetic energy distributions are developed for various combinations of amplifying and non-amplifying modes. The limit for large amplifications is a gaussian kinetic energy distribution. The limit for no amplification is a maxwellian-like distribution. Thus the formalism comprehends the fission decay on one hand and the neutron evaporation on the other. The angular distributions are evaluated in terms of the ridge-line principal moments of inertia. A general analytical expression has been derived which predicts, correctly in both limits, the angular distributions of the evaporated neutrons and of the fission fragments.

---

*Work done under the auspices of the U.S. Energy Resources Development Administration

†Sloan Fellow 1974-1976.

1. INTRODUCTION

The statistical decay of the compound nucleus at relatively low excitation energies occurs in the form of particle evaporation and of fission. In the first case, very light particles are emitted, like neutrons, protons, alpha particles; in the second case, very sizable fragments of approximately half the mass of the compound nuclei are observed. Such a dichotomy is stressed in the formalisms commonly used in the calculation of the decay widths. The standard evaporation formalism[1-4]) makes use of the detailed balance principle to connect the compound system with the decayed system at infinite separation of the two fragments (e.g., neutron and residual nucleus). The direct transition probability is obtained from the phase space volumes associated with the initial and final states and from the inverse transition probability deduced from an optical model.

The fission decay formalism, like the Bohr-Wheeler formalism,[5]) takes advantage of the saddle point in the nuclear potential energy as a function of deformation. At this point, which separates the compound nucleus region from the region of the forming fragments, there is a phase space constriction which controls the probability flow between the two regions. Furthermore, the direct and inverse transition probabilities are trivially related to the velocity of the system along the fission coordinate.

This apparent distinction between evaporation and fission is rather artificial. From the experimental standpoint, particles with mass intermediate between the fission fragments and the alpha particles have been

observed in high energy reactions[6-8]), and their cross section appears to increase rapidly with excitation energy[6]). In fact the high energy and angular momentum deposition associated with heavy ion reactions should raise these particles from the limbo of immeasurably low cross sections into the more accessible region of ordinary cross sections, thus making these processes open to experimental investigation.

From a theoretical standpoint, the inherent unity of the two processes can be easily shown. In this paper a special effort will be dedicated to a detailed description of the emission of intermediate particles. An attempt will be made to treat this problem on very general grounds, by trying to describe and classify the most relevant aspect of the physics in a manner which is as independent as possible from detailed models. Specific models will be used only for the purpose of exemplification. The emission probabilities, the kinetic energy distributions as well as the angular distributions will be calculated analytically. At the same time the features of the formalism which portray the essential unity of the statistical decay process will be stressed.

Part of this work has been published elsewhere in preliminary form[9]).

2. POTENTIAL ENERGY ASPECTS: THE RIDGE LINE

The nuclear potential energy surface $V(x_i)$ as a function of a set of deformation coordinates x_i has been studied in detail by making use of the liquid drop model[10-12]). The stationary points of this surface can be obtained by solving the system of equations:

$$\frac{\partial V(x_i)}{\partial x_i} = 0$$

In general, only the solutions of the above equations are the part of the topology which is invariant with respect to a canonical transformation of coordinates. In particular the ground state and the fission saddle point are independent of the representation which is chosen, while the overall topology of the potential energy depends upon the choice of the coordinates. However, it is well known that the saddle point shapes for values of the fissility parameter $x \leqslant 0.7$ are strongly constricted at the neck, so that the two forming fission fragments are already well defined in their masses A_1 and A_2. In this way a mass asymmetry parameter $\frac{A_1}{A_1 + A_2}$ can be defined. This feature of the saddle point shape has been employed by Nix[12]) who introduced a particularly simple parameterization of saddle point shapes in terms of two touching spheroids. In the limit in which the mass asymmetry is a well defined quantity, it is possible to consider a cut of the potential energy surface along the mass asymmetry coordinate passing through the saddle point and such that, at any point of this cut, the potential energy is stationary with respect to all other coordinates. Each point on this line is then a saddle point with the constraint of a fixed mass asymmetry. In analogy with the name "saddle point", we may call this line "ridge line". In the limit of large mass asymmetries, the two spheroid parameterization is expected to be a good approximation even for values of the fissility parameters larger than 0.7. Furthermore, for very large mass asymmetries, the small fragment can be approximated by a sphere, thus simplifying the problem substantially.

The potential energy along the ridge line is shown in the two spheroid approximations for three nuclei (fig. 1). In fig. 2, the potential energy about the ridge point is plotted as a function of the deformation of the two spheroids. The two spheroids are colinear and in contact. In the same figure the Coulomb interaction energies of the two spheroids are shown.

3. STATISTICAL PARTITION AT THE RIDGE POINT AND TOTAL DECAY WIDTH

Assuming that the inertia tensor is known for the collective modes at the ridge point, a simultaneous diagonalization of the potential and kinetic energy expressions in the quadratic approximation is possible, thus leading to the definition of the normal modes at the ridge point. In the limit of complete uncoupling between collective and intrinsic modes, the decay width $\Gamma^{(n)}$, differential in n variables, can be written as:

$$\Gamma^{(n)} d\varepsilon dy dp_y \prod dx_i dp_i = \frac{1}{2\pi\rho(\varepsilon)} \rho^* \left[E - B_R(y) - \varepsilon - \frac{p_y^2}{2m_y} - \sum \left(a_i x_i^2 + \frac{p_i^2}{2m_i} \right) \right] \times \frac{dy dp_y}{h} \, d\varepsilon \prod \left(\frac{dx_i dp_i}{h} \right) \tag{1}$$

where x_i, p_i are the normal mode's coordinates and conjugate momenta; y and p_y are the mass asymmetry coordinate and momentum; $B_R(y)$ is the ridge point potential energy; ε is the kinetic energy of the fission-like mode; a_i and m_i are the stiffnesses and the inertias associated with the normal modes; $\rho(E)$ is the compound nucleus level density; $\rho^*[....]$ is the density of the intrinsic states at the ridge point.

If the collective degrees of freedom are coupled to the intrinsic

modes, or in other words, if the motion along the collective coordinates is viscous, then the form of the ridge phase-space is more difficult to define. Certainly the phase-space associated with the collective momenta is going to be limited by the fact that viscosity will prevent the system from attaining high velocities. This may have a great importance in the determination of the kinetic energy distributions, as will be seen later.

By expanding the natural logarithm of the ridge point level density in first order with respect to its argument, one obtains a rather accurate and very useful approximation:

$$\Gamma^{(n)} d\varepsilon dy dp_y \prod dx_i dp_i = \frac{1}{2\pi} \frac{\rho^*(E-B_R)}{\rho(E)} \exp - \frac{1}{T}\left[\varepsilon + \frac{p_y^2}{2m_y} + \sum\left(a_i x_i^2 + \frac{p_i^2}{2m_i}\right)\right] \times \frac{dy dp_y}{h} \; d\varepsilon \prod \frac{(dx_i dp_y)}{h} \qquad (2)$$

where $\frac{1}{T} = \left.\frac{d\ln\rho^*(x)}{dx}\right|_{x = E - B_R}$.

In this approximation energy is not conserved. Rather, the system is characterized by a constant temperature T which describes the equilibrium between the collective degrees of freedom and the far more numerous intrinsic degrees of freedom which act as a thermostat.

This expression is essentially identical to the differential decay width for the fission process.

Equation (2) can be integrated to give the total decay width:

$$\Gamma^1 dy = \frac{1}{2\pi} \frac{T\rho^*(E - B_R)}{\rho(E)} \frac{(2\pi T m_y)^{\frac{1}{2}}}{h} \prod\left(\frac{\pi T}{h}\sqrt{\frac{2m_i}{a_i}}\right) dy \quad . \qquad (3)$$

Since it is rather unlikely that the quantities m_i, a_i can be determined with sufficient accuracy, it may be wise to incorporate all of the phase-space associated with the bound collective modes into a new level density expression ρ_R. The decay width then becomes:

$$\Gamma^{\uparrow}dy = \frac{1}{2\pi} \frac{T\rho_R(E - B_R)}{\rho(E)} \frac{(2\pi T m_y)^{\frac{1}{2}}dy}{h} . \qquad (4)$$

This expression for large values of E can be written approximately as:

$$\Gamma^{\uparrow}dy = \frac{1}{2\pi} \frac{T(2\pi T m_y)^{\frac{1}{2}}dy}{h} \exp - \frac{B_R}{T} \qquad (5)$$

where the contribution of the mass asymmetry mode to the phase-space has been explicitly isolated. The leading factor in this expression is the exponential. The pre-exponential factor is hard to calculate because of the inertial parameter m_y. However, there is reason to expect that this term varies slowly with asymmetry y. Consequently we can estimate the yield of the statistically emitted fragments to within an approximately constant factor (fig. 1).

4. THE KINETIC ENERGY DISTRIBUTION; AMPLIFYING AND NON-AMPLIFYING MODES

In the case of charged particle evaporation, the greatest fraction of the kinetic energy of the particle at infinity originates from the Coulomb repulsion. Therefore great care must be taken in describing the shape of the system at the time of division, because the distance between the centroids of the two charges is critical in determining the Coulomb energy. In the present treatment, the relevant shape is that of the ridge

point, which, at all times, we consider degenerate with the scission configuration. As can be seen from the two spheroid model or from the spheroid-sphere model, the ridge point configuration can be substantially elongated (shape polarization of the two fragments) so that the distance between the centroids of the two charge distributions is larger than that of two touching spheres. Thus the Coulomb energy is smaller than the nominal Coulomb barrier (corresponding to two touching spheres), and apparent subCoulomb barrier emission may result. An indication of subCoulomb barrier emission is already available in ^{4}He evaporation[13,14]). This effect, which is ordinarily attributed to quantum mechanical barrier penetration, finds here a possible explanation which is entirely classical. A similar, but more pronounced effect, has been observed in the emission of complex particles from high energy bombardments[7,8]). The extreme limit of this effect is visible in the fission process where the kinetic energies are indeed substantially lower than the Coulomb energies of two touching spheres.

A second point, very relevant to this discussion, is the origin of the width of the kinetic energy distributions. In the case of neutron evaporation, the kinetic energy width originates from the statistical fluctuations associated with the neutron degrees of freedom (translational modes). In the case of charged particle emission, fluctuations in kinetic energy may also arise from fluctuations in various bound collective degrees of freedom. These shape fluctuations can contribute greatly to the kinetic energy fluctuation, as can be seen in the following example. Let us plot the ridge point potential energy for the sphere-spheroid model as a function of the spheroid deformation (fig. 3). On the same graph let

us plot the Coulomb interaction energy of the two touching fragments, also as a function of the spheroid deformation. In second order in the deformation parameter $z = \beta - \beta_{eq}$, the potential energy has the form:

$$V_T = V_R + kz^2 \tag{6}$$

while the Coulomb interaction energy in first order has the form:

$$V_c = E_o - cz \quad . \tag{7}$$

The fluctuation in potential energy associated with the deformation mode in equilibrium with a thermostat with temperature T is of the order $\frac{1}{2}$ T. The corresponding fluctuation in Coulomb energy is:

$$\sigma_c = \sqrt{\frac{c^2 T}{2k}} = \sqrt{\frac{pT}{2}} \tag{8}$$

where the parameter $p = c^2/k$ is dependent only upon the potential energy of the ridge point mode in question. The width σ_c for sufficiently large values of the parameter p may become the dominant contribution to the spread in kinetic energy. A pictorial way to explain such an amplification of a fluctuation is to compare the system in question to an amplifier. The input to the amplifier is a white noise of mean amplitude $\frac{1}{2}$ T. Because of the characteristics of the amplifier, an output signal of mean amplitude $\sqrt{pT/2}$ is emitted. The parameter p then can be properly called amplification parameter and a degree of freedom with such a general structure can be called *amplifying mode*. In general, a mode is amplifying when at various elongations (deformations) the relative contribution of

surface and Coulomb energy to the total potential energy changes widely.

At the other extreme we have *non-amplifying modes* when their potential energies arise almost exclusively from Coulomb energy. For instance the oscillation of the spherical small fragment about the tip of the large spheroidal fragment can be considered a non-amplifying mode. As the fragment rolls (or slides) away from the tip of the spheroid towards the equator, the Coulomb energy increases because of the decreasing distance between the two fragments, while the surface energy of the system changes only in higher order and can be considered approximately constant.

5. DETAILED EVALUATION OF THE FINAL KINETIC ENERGY DISTRIBUTIONS

A detailed expression for the kinetic energy distribution at infinity cannot be obtained without a well defined model for the ridge point degrees of freedom. In what follows we shall try to obtain results which are on one hand as simple as possible, on the other very general and dependent only upon the essential features of any specific model. The following assumptions will be made:

i) The ridge point modes are of three kinds, amplifying modes, non-amplifying modes, and one decay mode

ii) The decay mode and the non-amplifying modes contribute their total energy (potential and kinetic) to the final kinetic energy, while the amplifying modes contribute only the coulombic part of the potential energy.

Some justification of these assumptions can be found in the sphere-spheroid model or in the two spheroid models. In both of these models there is a fairly well defined separation of the ridge modes in the

amplifying and non-amplifying classes. Furthermore, the kinetic energy associated with the amplifying modes is mainly in the form of kinetic energy of vibration of the fragments and should not appear to any great extent in the final kinetic energy. In what follows, different combinations of the various kinds of degrees of freedom will be employed and various analytical expressions will be derived.

5.1. One Decay Mode and One Amplifying Mode

The decay width takes the following form:

$$\Gamma^{(4)}\,dy\,d\epsilon\,dz\,dp_z = \frac{dy\,(2\pi T m_y)^{\frac{1}{2}}\,\rho_R(E - B_R)}{h\ 2\pi\ \rho(E)}\ \exp - \frac{1}{T}\left(\epsilon + \frac{p_z^{\,2}}{2m_z} + V(z)\right)\frac{dz\,dp_z\,d\epsilon}{h} \tag{9}$$

In this expression z, p_z, m_z, and $V(z)$ are the coordinate, conjugate momentum, inertia and potential energy of the amplifying mode; ϵ is the kinetic energy of the decay mode.

Since the kinetic energy associated with the amplifying mode is not expected to contribute to the final kinetic energy, one can integrate directly over p_z. Furthermore, one can express $V(z)$ in the quadratic approximation:

$$V(z) = B_R + kz^2 \tag{10}$$

One then obtains:

$$\Gamma^{(3)}\,dy\,d\epsilon\,dz = \frac{dy\,(2\pi T m_y)^{\frac{1}{2}}}{h}\ \frac{\rho_R(E - B_R)}{2\pi\ \rho(E)}\ \frac{(2\pi m_z T)^{\frac{1}{2}}}{h}\ \exp\left[-\frac{1}{T}\,(\epsilon + kz^2)\right]d\epsilon\,dz \tag{11}$$

Let us now assume that the kinetic energy at infinity is given by:

$$E_k = E_{coulomb} + \varepsilon \cong E_o - cz + \varepsilon \tag{12}$$

where E_o is the Coulomb interaction energy at the ridge point and cz is its first order dependence upon the deformation parameter z. Then the kinetic energy distribution at infinity is:

$$P(E_k)dE_k \propto dE_k \int_0^{E_k} \exp - \frac{1}{T}\left\{\varepsilon + \frac{k}{c^2}(E_k - E_o - \varepsilon)^2\right\} d\varepsilon \tag{13}$$

where all the irrelevant multiplicative factors have been dropped. Letting $\frac{c^2}{k} = p$ and $E_k - E_o = x$ one obtains:

$$P(x)dx \propto \exp\left(-\frac{x}{T}\right)\left\{\operatorname{erf}\frac{2E_o + p}{2\sqrt{pT}} - \operatorname{erf}\frac{p - 2x}{2\sqrt{pT}}\right\}dx \quad . \tag{14}$$

Even for small charged particles, and rather large temperatures, the argument of the first error function is quite large. Consequently,

$$\operatorname{erf}\frac{2E_o + p}{2\sqrt{pT}} \simeq 1 \ ,$$

and (15)

$$P(x)dx \propto \exp\left(-\frac{x}{T}\right)\operatorname{erfc}\frac{p - 2x}{2\sqrt{pT}}\,dx \quad .$$

5.2. <u>One Decay Mode, One Amplifying Mode and One Non-Amplifying Mode</u>

Let us label the non-amplifying degree of freedom as t. The decay width can be written as:

$$\Gamma^{(5)}dyd\varepsilon dzdtdp_t = \frac{dy(2\pi Tm_y)^{\frac{1}{2}}}{h}\,\frac{\rho_R(E-B_R)}{2\pi\,\rho(E)}\,\frac{dz(2\pi m_z T)^{\frac{1}{2}}}{h}\,\frac{dtdp_t}{h}\exp - \left(\varepsilon + kz^2 + at^2 + \frac{p_t^2}{2m_t}\right)d\varepsilon \tag{16}$$

Since all the terms in ε, t, p_t contribute to the final kinetic energy, we can collect them, account for the associated phase-space and obtain:

$$P(E_k)dE_k \propto dE_k \int_0^{E_k} \ell \exp -\frac{1}{T}\left\{\ell + \frac{k}{c^2}(E_k - E_o - \ell)^2\right\} d\ell \qquad (17)$$

where one has set, as before:

$$E_k = E_o - cz + \ell \quad . \qquad (18)$$

After integration one obtains:

$$P(x)dx \propto \left\{(2x - p)\exp\left(-\frac{x}{T}\right)\left[\operatorname{erf}\frac{2E_o + p}{2\sqrt{pT}} - \operatorname{erf}\frac{p - 2x}{2\sqrt{pT}}\right]\right. \qquad (19)$$
$$\left. + \frac{2\sqrt{pT}}{\sqrt{\pi}}\left[\exp\left(-\frac{p^2 + 4x^2}{4pT}\right) - \exp\left(-\frac{(2E_o + p)^2 + 4px}{4pT}\right)\right]\right\} dx$$

Again, if $E_o >> \sqrt{pT}$, the above expression can be simplified as follows:

$$P(x)dx \propto \left\{(2x - p)\exp\left(-\frac{x}{T}\right)\operatorname{erfc}\frac{p - 2x}{2\sqrt{pT}} + 2\sqrt{\frac{pT}{\pi}}\exp\left(-\frac{p^2 + 4x^2}{4pT}\right)\right\} dx \qquad (20)$$

5.3. One Decay Mode, One Amplifying Mode and Two Non-Amplifying Modes

Equation (17), with the addition of one extra non-amplifying mode, becomes:

$$P(E_k)dE_k \propto dE_k \int_0^{E_k} \ell^2 \exp -\frac{1}{T}\left\{\ell + \frac{k}{c^2}(E_k - E_o - \ell)^2\right\} d\ell \qquad (21)$$

where one has employed the usual expression for the kinetic energy. After integration one obtains:

$$P(x)dx \propto \left\{\left(\tfrac{1}{4}p^2 + \frac{pT}{2} + x^2 - px\right)\exp\left(-\frac{x}{T}\right)\left[\operatorname{erf}\frac{2E_o + p}{2\sqrt{pT}} - \operatorname{erf}\frac{p - 2x}{2\sqrt{pT}}\right]\right.$$

$$\left. + \frac{\sqrt{pT}}{2\sqrt{\pi}}\left[(2x - p)\exp\left(-\frac{p^2 + 4x^2}{4pT}\right) - (2E_o + p)\exp\left(-\frac{(2E_o + p)^2 + 4px}{4pT}\right)\right]\right\}dx$$

Again, if $E_o >> \sqrt{pT}$ the above expression becomes:

$$P(x)dx \propto \left\{\left(\tfrac{1}{4}p^2 + \frac{pT}{2} + x^2 - px\right)\exp\left(-\frac{x}{T}\right)\operatorname{erfc}\frac{p - 2x}{2\sqrt{pT}}\right.$$

$$\left. + \frac{\sqrt{pT}}{2\sqrt{\pi}}(2x - p)\exp\left(-\frac{p^2 + 4x^2}{4pT}\right)\right\}dx \qquad (23)$$

6. COMMENTS ON THE FEATURES OF THE KINETIC ENERGY DISTRIBUTION EXPRESSIONS AND THEIR ASYMPTOTIC LIMITS

The first observation one can make about the three equations derived above concerns the different way in which the amplifying and the non-amplifying modes manifest themselves. The amplifying mode affects the kinetic energy distribution through the amplification parameter p, which depends upon the potential energy features of the system at the ridge point. The non-amplifying modes affect the kinetic energy distribution only through their number and not through any feature related either to the potential energy or to the inertia.

The second observation deals with the most probable values and the width of the kinetic energy distribution at constant values of p. As can be seen from fig. 4, the most probable energy shift towards higher values as the number of non-amplifying modes increases. For sufficiently large values of p, the width of the distribution is essentially determined by p and increases slightly with increasing number of non-amplifying modes.

In all the cases, but especially at large values of p, a substantial fraction of the kinetic energy distribution occurs below the nominal Coulomb barrier (fig. 4). Again, this effect in the present model arises simply from classical factors associated with shape polarization and statistical fluctuations at the ridge point. It has nothing to do with quantum mechanical penetration of the barrier, which has not been included in the model.

A third aspect of this calculation has to do with the general appearance of the kinetic energy spectra. All of the three equations predict a highly asymmetric, maxwellian-like shape for small values of p (fig. 4). This can be seen best in Eq. (20) and Eq. (23). At small p values the first term, containing erfc, dominates, giving rise to a strong asymmetry. At large values of p the term containing erfc tends to zero and the second term, which is a gaussian, dominates.

6.1. Limiting Expressions for p = 0

First, let us consider the limit to which the three expressions, Eqs. (15), (20), and (23), tend when the amplification parameter p tends to zero. This occurs when the charge of the emitted particle goes to zero. Under these conditions $x \equiv E_k$. By noticing that in this limit the function erfc tends to a non-zero constant $\left[\lim_{x \to \infty} \text{erfc}(-x) = 2\right]$ one obtains:

$$P(E_k)dE_k \propto \begin{cases} \exp - E_k/T & (24a) \\ E_k \exp - E_k/T \quad dE_k & (24b) \\ E_k^2 \exp - E_k/T & (24c) \end{cases}$$

It appears that one can write a general expression as:

$$P(E_k)dE_k \propto E_k^n \exp - E_k/T \quad dE_k \tag{25}$$

where n is the number of non-amplifying degrees of freedom. The exact meaning of the limit $p \to 0$ can only be determined from a specific model. In the case of the sphere-spheroid model, the non-amplifying modes, corresponding to the oscillation of the sphere about the tip of the spheroid, become unbound since the charge of the light particle goes to zero and the shape polarization of the large fragment vanishes. In the case in which a non-amplifying mode becomes unbound, the partition function loses one quadratic term in the coordinate but retains the quadratic term in the momentum. On the other hand this does *not* happen automatically in our formalism where we always *assume* the presence of quadratic terms associated with both the coordinate and the momentum for each mode.

Consequently if one considers the *two* degenerate non-amplifying modes associated with the oscillation of a small sphere about the tip of the spheroid, one should use the *third* kind of equation [Eq. (24c)] if $p > 0$. On the other hand, for $p = 0$ one should use instead the limiting form of the *second* kind of equation, namely Eq. (24b). The case of neutron emission can well be described as the limiting case of two non-amplifying modes. As was shown above, the proper limiting form is Eq. (24b) which is similar to a maxwellian. The same prediction is obtained from more conventional theories. A detailed description of the smooth transition from charged particle emission to neutron emission requires the knowledge of the onset of anharmonicities in the non-amplifying modes at potential energies larger than T. This can only be done by investigating a specific model and goes beyond the scope of this paper.

6.2 Limiting Expressions for Large Amplification Parameters and for More than One Amplifying Mode

Large amplification parameters are expected for systems with large atomic number emitting rather large fragments. As can be seen in fig. (4), the contribution of the decay mode and of the non-amplifying modes to the kinetic energy distribution becomes less and less important as p increases. This is particularly evident in the tendency of the kinetic energy distribution to become more symmetrical and nearly gaussian at large values of p. In these cases, more than one amplifying mode may be present and the two spheroid model with two amplifying modes may be more appropriate than the sphere-spheroid model. If, for the moment, one overlooks the contribution of the decay mode and of the non-amplifying modes to the

mean and to the width of the final kinetic energy distribution, one can easily calculate the kinetic energy distribution resulting from two amplifying modes. Let the two amplifying modes be ξ and η. The probability of deformation of the system is:

$$P(\xi,\eta)d\xi d\zeta \propto \exp -\frac{1}{T}(k_1\xi^2 + k_2\eta^2)\, d\xi d\eta \tag{26}$$

where k_1 and k_2 are the stiffnesses of the two normal modes. The total kinetic energy can be written as:

$$E_k = E_o - c_1\xi - c_2\eta \tag{27}$$

By substituting Eq. (27) into Eq. (26) and integrating over all the possible configurations leading to the same kinetic energy, one obtains:

$$P(x)dx \propto \exp -\frac{x^2}{(p_1 + p_2)T}\, dx \tag{28}$$

where $x = E_k - E_o$ and $p_1 = \frac{c_1^2}{k_1}$ and $p_2 = \frac{c_2^2}{k_2}$.

This result can be easily generalized to any number of amplifying modes:

$$P(x)dx \propto \exp -\frac{x^2}{T\sum p_i}\,. \tag{29}$$

In other words the kinetic energy is a gaussian of width $\sigma^2 = \frac{1}{2}\sum p_i T$.

The effect of the decay mode and of the non-amplifying modes on the mean and the width of the kinetic energy distribution can be estimated as follows. The mean kinetic energy associated with one decay mode and n non-amplifying modes is:

$$\bar{\varepsilon} = \frac{\int_0^\infty \varepsilon^{n+1} \exp(-\varepsilon/T)d\varepsilon}{\int_0^\infty \varepsilon^{n} \exp(-\varepsilon/T)d\varepsilon} = (n+1)T \quad . \tag{30}$$

The corresponding width can be written as:

$$\sigma^2 = \frac{\int_0^\infty (\varepsilon-\bar{\varepsilon})^2 \varepsilon^{n} \exp(-\varepsilon/T)d\varepsilon}{\int_0^\infty \varepsilon^{n} \exp(-\varepsilon/T)d\varepsilon} = (n+1)T^2 \quad . \tag{31}$$

Therefore the kinetic energy distribution can be written down more accurately as:

$$P(x)dx \propto \exp - \frac{x^2}{(p_1 + p_2)T + 2(n+1)T^2} dx \tag{32}$$

where $x = E_k - E_o - (n+1)T$.

6.3. Angular Momentum Effects in the Kinetic Energy Distributions

The generalization of the formalism to the case of a given non-zero angular momentum is straightforward. The ridge potential energy is modified to include the rotational energy of the system at the ridge. This involves the evaluation of the ridge moment of inertia as a function of the deformation coordinates. In the case of a single amplifying mode, a constant k, analogous to that defined in Eq. (6) can be introduced. The kinetic energy at infinity depends both upon the Coulomb energy as well as upon the rotational kinetic energy associated with the orbital angular momentum of the two touching fragments. One can then define the following quantity:

$$V^* = V_c + \tfrac{1}{2}\mu r^2 \omega^2 \tag{33}$$

where μ is the reduced mass of the two fragments in contact; r is the distance between the centroids of the two fragments; ω is the angular velocity of the system defined by

$$I = \omega\mathscr{I} = \omega(\mathscr{I}_1 + \mathscr{I}_2 + \mu r^2) \tag{34}$$

In this expression I is the total angular momentum and $\mathscr{I}_1, \mathscr{I}_2$ are the moments of inertia of the two fragments. As in Eq. (7), one can expand V^* as follows:

$$V^* = E_o^* - cz \tag{35}$$

This equation defines the quantity c and an amplification parameter $p = c^2/k$ can be introduced. All the previous expressions can now be used provided one redefines x as $x = E_k - E_o^*$. The definition of temperature also must account for the kinetic energy tied up in the form of rotational energy at the ridge:

$$\frac{1}{T} = \frac{d\ell n\rho^*(x)}{dx}\Bigg|_{x = E - B_R - E_{rot}}$$

The resulting kinetic energy distributions for a fixed I must then be integrated over the angular momentum distribution of the compound nucleus.

7. THE ANGULAR DISTRIBUTIONS

The ridge point configuration, for the great majority of cases, can be identified with the scission configuration. Furthermore, the disintegration axis and the symmetry axis of the system at the ridge point should approximately coincide. As a consequence, the projection K of the total angular momentum I on the symmetry/disintegration axis should remain constant from the ridge point to infinity. Such a condition implies a relation between the total angular momentum and the orbital angular momentum of the two fragments, thus determining the final angular distribution. This approach is similar to the theory of fission fragment angular distribution[15]). In the fission theory, the assumption of constant K from saddle to infinity is somewhat uncertain, especially for very heavy elements, due to the complicated dynamical evoluation leading from saddle to scission. In our case, due to the closeness of the ridge and the scission points, the theory ought to work even better than in fission.

The differential cross section can be written as follows[16]):

$$\frac{d\sigma}{d\Omega} = \int_0^{I_{max}} dI\ \sigma_I \int_{-I}^{+I} dK \frac{\Gamma_f^I(K)}{\Gamma_T^I}\ W_K^I(\theta) \tag{36}$$

where

$$\Gamma_f^I(K) = \frac{\Gamma_f^o}{2I+1}\ \exp\left[-\frac{\hbar^2 I^2}{2T}\left(\frac{1}{\mathcal{I}_1} - \frac{1}{\mathcal{I}_c}\right)\right] \exp\left(-K^2/2K_o^2\right) \tag{37}$$

σ_I is the reaction cross section for the I^{th} partial wave, and $W_K^I(\theta)$ can be written in the classical limit as:

$$W_K^I(\theta) \propto \frac{2I + 1}{\sqrt{\sin^2\theta - \frac{K^2}{I^2}}} \tag{38}$$

In Eq. (37) $\mathscr{I}_c$ is the compound nucleus moment of inertia; K_o^2 is the standard deviation of the statistical distribution of K values and is given by:

$$K_o^2 = \frac{\mathscr{I}_{eff}\, T}{\hbar^2} \tag{39}$$

The quantity $\mathscr{I}_{eff}$ is related to the principal moments of inertia, $\mathscr{I}_\parallel$ and $\mathscr{I}_\perp$, of the system at the ridge point by the relation:

$$\frac{1}{\mathscr{I}_{eff}} = \frac{1}{\mathscr{I}_\parallel} - \frac{1}{\mathscr{I}_\perp} \tag{40}$$

It is worth considering that, at fixed temperature T, the width of the K distribution becomes broader as the ridge configuration becomes more compact.

If one assumes that $\Gamma_T \simeq \Gamma_n$, the integration over K of Eq. (36) gives:

$$W(\theta) \propto \int_0^{I_{max}} \frac{2I dI \exp\left(-\frac{I^2\sin^2\theta}{4K_o^2}\right) I_0\left(\frac{I^2\sin^2\theta}{4K_o^2}\right)}{\exp - \beta I^2} \tag{41}$$

In this expression I_0 is the modified Bessel function of order 0 and

$$\beta = \frac{\hbar^2}{2T}\left(\frac{1}{\mathscr{I}_n} - \frac{1}{\mathscr{I}_\perp}\right) \quad , \tag{42}$$

$\mathcal{I}_n$ being the moment of inertia of the residual nucleus after neutron emission. If $\beta I^2 \ll 1$ then $\exp - \beta I^2 \simeq 1$ and the integral becomes of the form:

$$W(\theta) \propto \frac{1}{\sin^2\theta} \int_0^{z_{max}} \exp(-z) I_0(z) dz = \frac{z_{max}}{\sin^2\theta} \exp(-z_{max}) \left(I_0(z_{max}) + I_1(z_{max}) \right) \tag{43}$$

where $z = \frac{I^2 \sin^2\theta}{4K_o^2}$, $z_{max} = \frac{I_{max}^2 \sin^2\theta}{4K_o^2}$, and I_0, I_1 are the modified Bessel functions of order 0, 1. Explicitly, one obtains:

$$W(\theta) \propto \exp\left(- \frac{I_{max}^2 \sin^2\theta}{4K_o^2} \right) \left[I_0 \left(\frac{I_{max}^2 \sin^2\theta}{4K_o^2} \right) + I_1 \left(\frac{I_{max}^2 \sin^2\theta}{4K_o^2} \right) \right] \tag{44}$$

In order to obtain a better accuracy one can expand the denominator to higher order:

$$e^{\beta I^2} \sim 1 + \beta I^2 \tag{45}$$

In many cases, for large temperatures, such an expansion ought to be adequate even at rather large angular momenta. The angular distribution becomes then:

$$\begin{aligned} W(\theta) \propto & \exp(-z_{max}) \left[I_0(z_{max}) + I_1(z_{max}) \right] \\ & + \frac{\beta I_{max}^2}{2} \exp(-z_{max}) \left[I_o(z_{max}) + 2/3\, I_1(z_{max}) - 1/3\, I_2(z_{max}) \right] \end{aligned} \tag{46}$$

This expression has two interesting limits: as $p = \frac{I_{max}^2}{4K_o^2}$ tends to infinity (either because K_o^2 tends to zero or because

I_{max} becomes very large) one can use the asymptotic expression for the Bessel functions:

$$I_\nu(z) = \frac{e^z}{\sqrt{2\pi z}} \left(1 - \frac{4\nu^2 - 1}{8z} + \ldots.\right) \tag{47}$$

Then if one keeps only the lowest term in the $z^{-\frac{1}{2}}$ expansion one obtains:

$$\lim_{p \to \infty} W(\theta) \propto \frac{1}{\sin\theta} \tag{48}$$

On the other hand, as $p \to 0$ (either because $I_{max} \simeq 0$ or $K_o^2 \to \infty$) one obtains:

$$\lim_{p \to \infty} W(\theta) = \text{constant} \quad . \tag{49}$$

These two limits represent the two extreme cases for the coupling between total and orbital angular momentum. The coupling is maximum in the first case and non-existent in the second case. Clearly the coupling parameter p depends upon the principal moments of inertia of the ridge configuration. This allows one to make a very simple prediction. At constant I_{max}, p becomes larger the bigger the difference between $\mathcal{I}_\parallel$ and $\mathcal{I}_\perp$, or in other words, the more elongated the ridge configuration is. Thus the anisotropy W(0)/W(90) will progressively increase as one considers the emission of a neutron, an alpha particle, a lithium particle, a berillium particle, etc. (see fig. 5). It is amusing to notice that Eq. (46) gives reasonable predictions for the angular distribution of neutrons as well. The ridge point configuration for the neutron emission is represented by a neutron just outside the nucleus. The principal moments of inertia can be approximately expressed as follows:

$$\mathscr{I}_{\parallel} \simeq \mathscr{I} \qquad \mathscr{I}_{\perp} \simeq \mathscr{I} + \mu R^2 \tag{50}$$

where $\mathscr{I}$ is the moment of inertia of the residual nucleus, μ is the reduced mass of the neutron nucleus system and R is the distance between neutron and nucleus when they are in contact. In many cases $\mathscr{I} >> \mu R^2$. Thus the quantity z takes the approximate form:

$$z = \frac{\hbar^2 I_{max}^2 \sin^2\theta}{4T}\left(\frac{1}{\mathscr{I}_{\parallel}} - \frac{1}{\mathscr{I}_{\perp}}\right) \simeq \frac{\hbar^2 I_{max}^2 \sin^2\theta}{4T\mathscr{I}}\left(1 - \frac{1}{1 + \frac{\mu R^2}{\mathscr{I}}}\right)$$

$$\simeq \frac{\hbar^2 I_{max}^2 \sin^2\theta}{4T\mathscr{I}} \frac{\mu R^2}{\mathscr{I}} = \frac{\bar{E}_R}{T} \frac{\mu R^2}{\mathscr{I}} \sin^2\theta \tag{51}$$

where $\bar{E}_R$ is the mean rotational energy of the residual nucleus. Similarly,

$$\mathscr{I}_c \simeq \mathscr{I}_{\parallel} \simeq \mathscr{I} \qquad \text{and} \qquad \tfrac{1}{2}\beta I^2 = \frac{z}{\sin^2\theta} = \frac{\bar{E}_R}{T} \frac{\mu R^2}{\mathscr{I}} = \alpha$$

Expanding Eq. (46) to first order in z we obtain:

$$W(\theta) \simeq 1 - \tfrac{1}{2} z + \tfrac{1}{2}\beta I_{max}^2 (1 - \tfrac{2}{3} z) \simeq 1 + \frac{\bar{E}_R}{T} \frac{\mu R^2}{\mathscr{I}} - \tfrac{1}{2} \frac{\bar{E}_R}{T} \frac{\mu R^2}{\mathscr{I}} \sin^2\theta$$

$$= 1 + \alpha - \tfrac{1}{2}\alpha \sin^2\theta \tag{53}$$

The normalized angular distribution in first order takes the form:

$$\frac{W(\theta)}{W(90)} = \frac{1 + \alpha - \tfrac{1}{2}\alpha \sin^2\theta}{1 + \tfrac{1}{2}\alpha} \simeq (1 - \tfrac{1}{2}\alpha)(1 + \alpha - \tfrac{1}{2}\alpha \sin^2\theta)$$

$$= 1 + \tfrac{1}{2}\alpha \cos^2\theta = 1 + \tfrac{1}{2} \frac{\bar{E}_R}{T} \frac{\mu R^2}{\mathscr{I}} \cos^2\theta$$

The very same normalized distribution has been obtained by Ericson from a more conventional evaporation theory[17]).

8. CONCLUSION

The formalism developed in this paper allows one to describe the decay of a highly excited compound nucleus by the emission of a sizable fragment. The only limitation of the formalism lies in the assumption that the ridge point and the scission point coincide. Such an approximation is adequate for fragments as large as fission fragments for compound nuclei with $x \leqslant .7$. For compound nuclei of larger x values the approximation is only satisfied for progressively larger asymmetries. The kinetic energy distributions can be expressed in terms of one or more amplification parameters obtained from the potential energy surface, and from a single statistical parameter, the nuclear temperature. Similarly the angular distributions are calculated from the principal moments of inertia at the ridge, from the temperature and from the angular momentum distribution. The amplification parameters and the moments of inertia can, but need not, be determined from the liquid drop model.

REFERENCES

[1] V. F. Weisskopf, Phys. Rev. 52 (1937) 295.

[2] V. F. Weisskopf, Helv. Phys. Acta 23 (1950) 187.

[3] V. F. Weisskopf, Proc. Acad. Arts Sci. 82 (1953) 360.

[4] V. F. Weisskopf and D. H. Ewing, Phys. Rev. 57 (1940) 472.

[5] J. A. Wheeler, "Channel Analysis of Fission" in Fast Neutron Physics Part II. (Interscience Publishers, 1963), p. 2051 and references therein.

[6] A. A. Caretto, J. Hudis, and G. Friedlander, Phys. Rev. 110 (1958) 1130.

[7] A. M. Poskanzer, G. W. Butler, and E. K. Hyde, Phys. Rev. C3 (1971) 882.

[8] E. K. Hyde, G. W. Butler, and A. M. Poskanzer, Phys. Rev. C5 (1971) 1795.

[9] L. G. Moretto, Physics Lett. 40B (1972) 185.

[10] S. Cohen, F. Plasil, and W. J. Swiatecki, Proceedings, Third Conf. on Reactions Between Complex Nuclei, editors A. Ghiorso, R. M. Diamond and H. E. Conzett, (University of California Press, 1963), p. 325; University of California Radiation Laboratory Report UCRL-10775 (1963).

[11] S. Cohen, F. Plasil and W. J. Swiatecki, University of California Berkeley Radiation Laboratory LBL-1502 (1972).

[12] J. R. Nix and W. J. Swiatecki, Nucl. Phys. 71 (1965) 1.

[13] J. Muto, H. Itoh, K. Okano, N. Shiomi, K. Fukuda, Y. Omori, and M. Kihara, Nucl. Phys. 47 (1963) 19.

[14] G. Chenevert, I. Halpern, B. G. Harvey, and D. L. Hendrie, Nucl. Phys. A112 (1968) 481.

[15]) I. Halpern and V. Strutinski, Proceedings of the Second Internat'l. Conf. on the Peaceful Uses of Atomic Energy, (Geneva, 1958), 15, p. 408.

[16]) G. N. Smirenkin and A. S. Tishin, Yad. Fiz. 12 (1970) 746; Sov. J. Nucl. Phys. 12 (1971) 403.

[17]) T. Ericson, Advan. Phys. 9 (1960) 425.

FIGURE CAPTIONS

Fig. 1. Ridge line potential energies and corresponding relative yields for three systems. The potential energies have been calculated by means of the two touching spheroid model. The yields have been calculated by assuming T = 2.0 MeV.

Fig. 2. Total potential energies and Coulomb interaction energies in the ridge point region as a function of the deformation of two touching spheroids. The energies are in MeV. The deformations DEF1, DEF2 refer to the large and small fragment respectively. The deformation parameters are defined as the ϵ_2 deformation in the recent Nilsson papers. The two orthogonal arrows center at the ridge point and are in the direction of the principal axes of the lowest constant energy ellipse. The light fragments are chosen with the same charge to mass ratio as the compound nucleus.

Fig. 3. Potential energy and Coulomb interaction energy as a function of the deformation of the large fragment (sphere-spheroid model). The thermal fluctuations about the ridge point result in largely amplified fluctuations in the Coulomb repulsion energy.

Fig. 4. Kinetic energy distributions at various temperatures for different values of the amplification parameter p. The three analytical expressions derived in the text have been employed. The curves corresponding to Eqs. (15), (20), (23) can be identified by their progressive shift towards higher kinetic energies. The arrows indicate the energies corresponding to the nominal Coulomb energies.

Fig. 5. Angular distributions of various fragments emitted by the compound nucleus formed in the reaction ^{208}Pb + 200 MeV $^{4}He \rightarrow {}^{212}Po$.

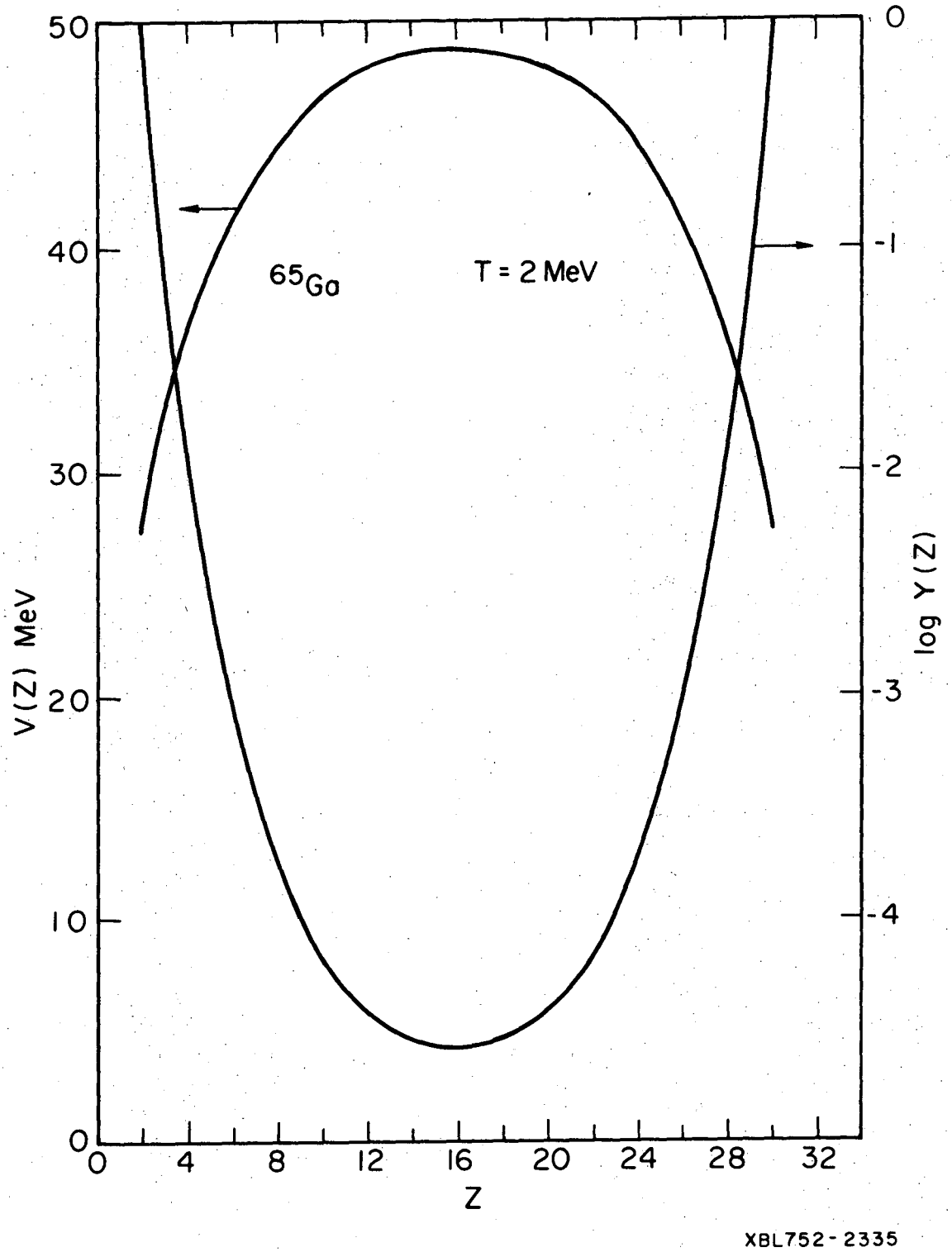
50
40
30
20
10
0
V(Z) MeV
0
4
8
12
16
20
24
28
32
Z
0
-1
-2
-3
-4
log Y(Z)
^{65}Ga
T = 2 MeV
XBL752-2335

Fig. 1a

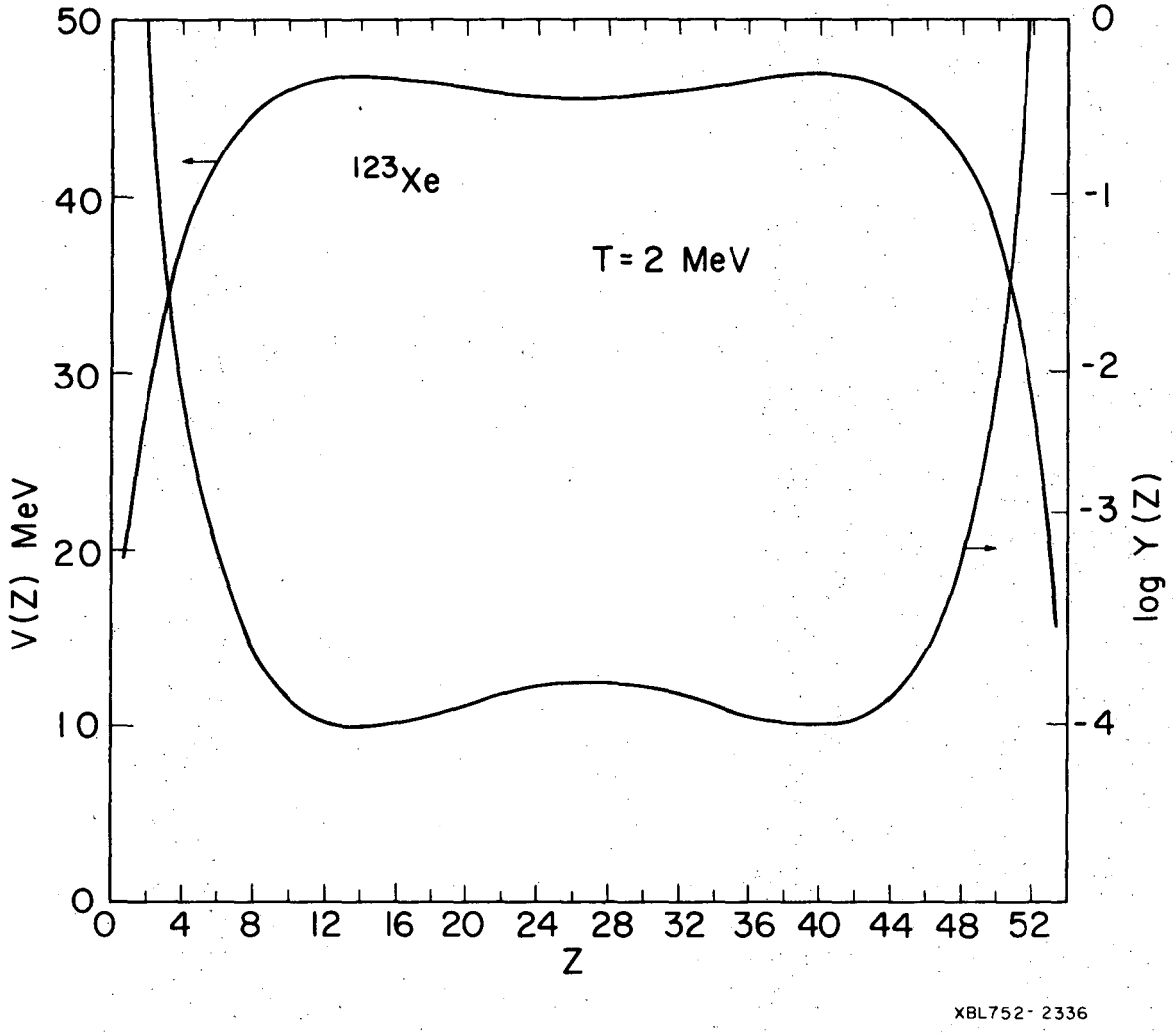
50
40
30
20
10
0
V(Z) MeV
0
-1
-2
-3
-4
log Y(Z)
^{123}Xe
T = 2 MeV
0 4 8 12 16 20 24 28 32 36 40 44 48 52
Z
XBL752-2336

Fig. 1b

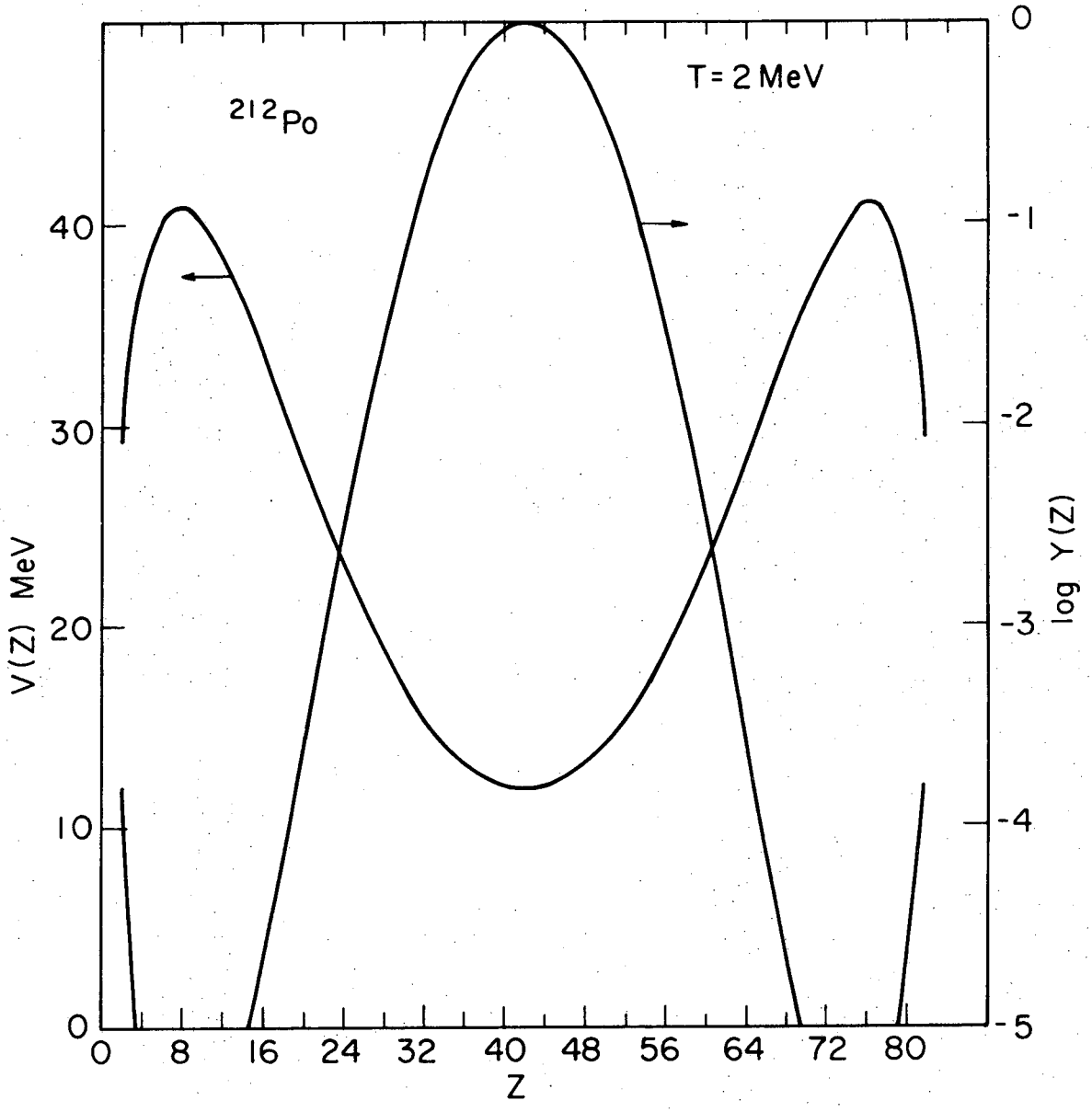
T = 2 MeV
212Po
V(Z) MeV
log Y(Z)
Z
0
8
16
24
32
40
48
56
64
72
80
0
10
20
30
40
-1
-2
-3
-4
-5
XBL752-2334

Fig. 1c

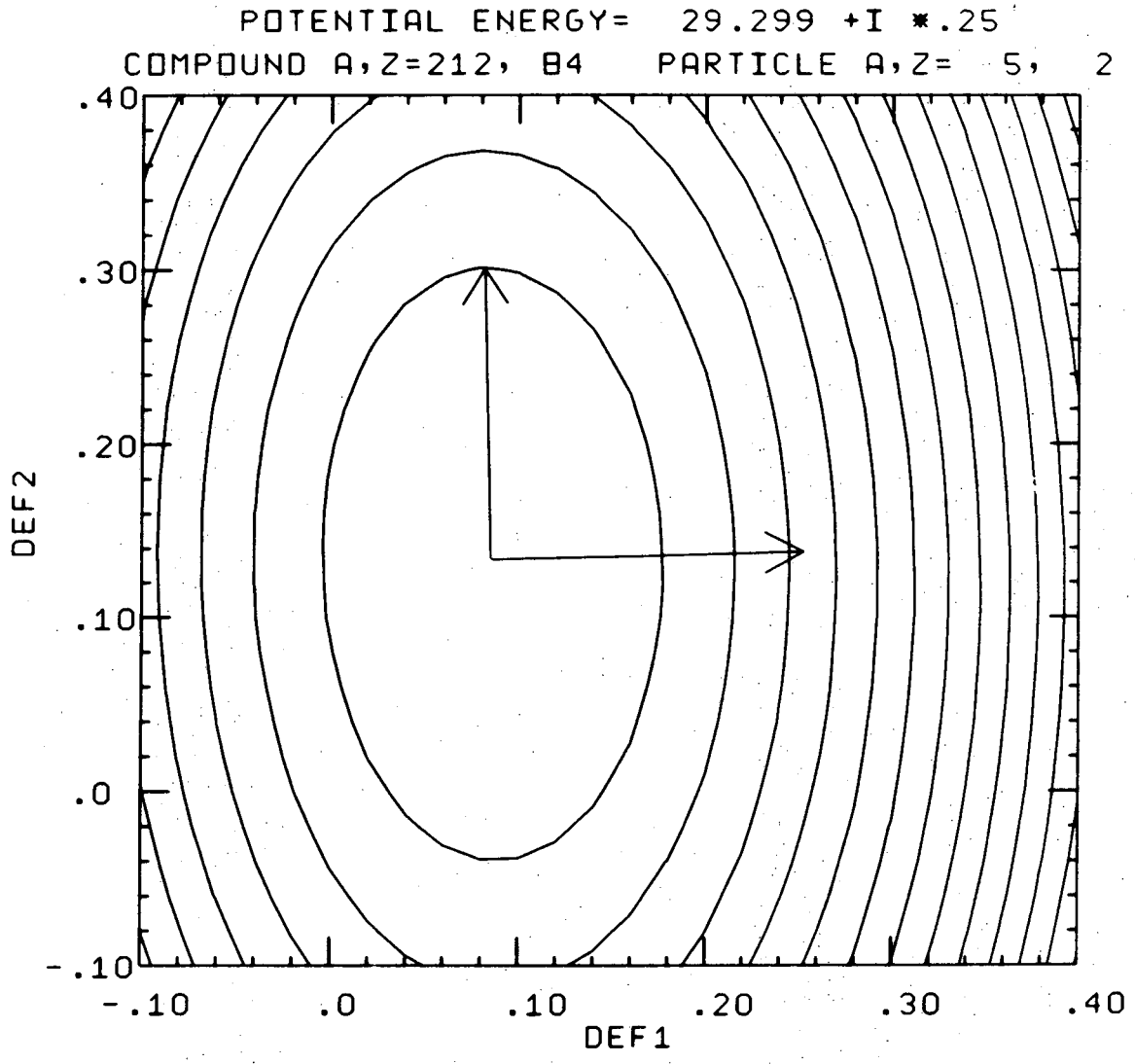
POTENTIAL ENERGY= 29.299 +I *.25
COMPOUND A,Z=212, 84 PARTICLE A,Z= 5, 2
.40
.30
.20
.10
.0
-.10
DEF2
-.10
.0
.10
.20
.30
.40
DEF1

Fig. 2a

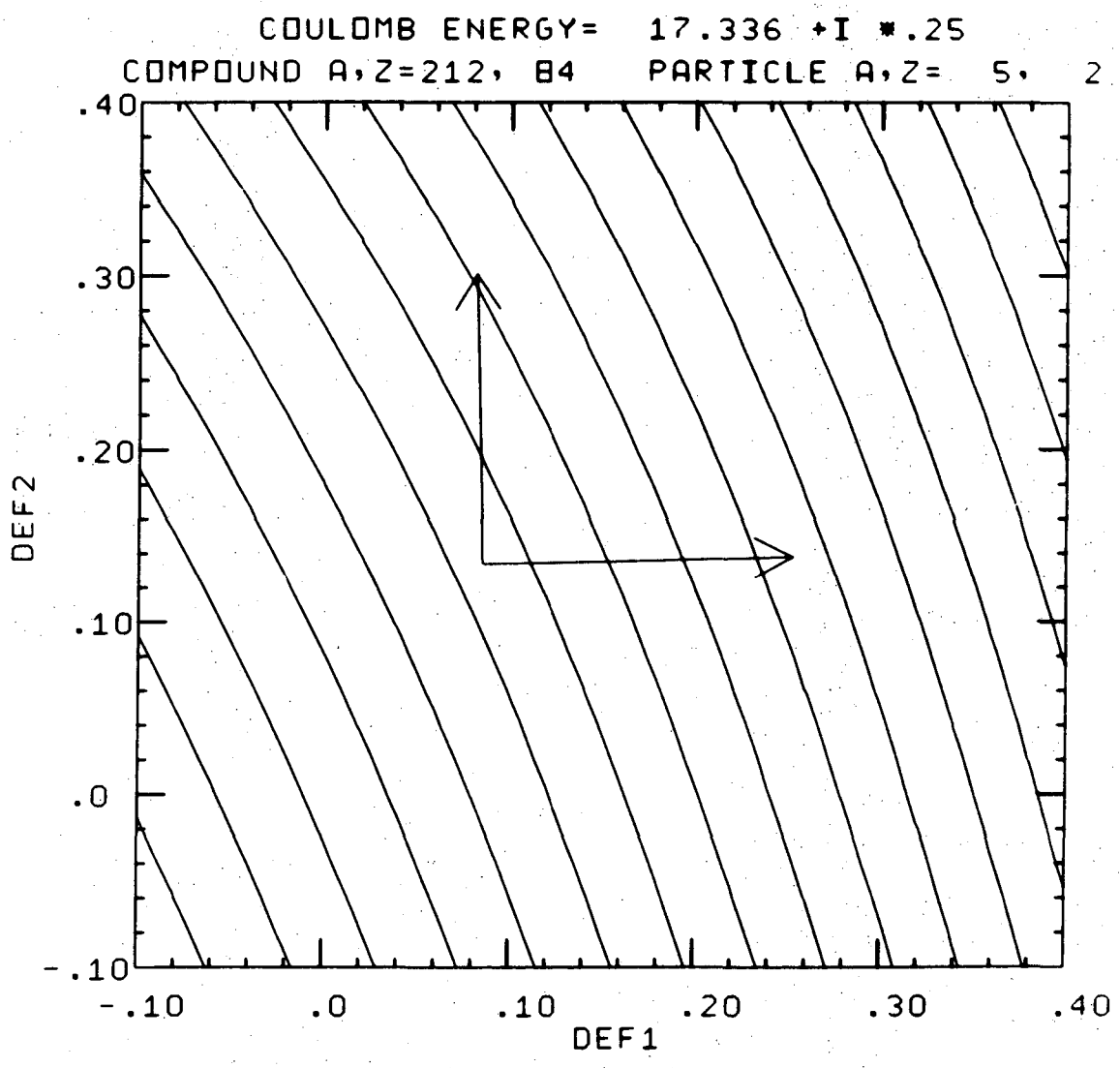
COULOMB ENERGY= 17.336 +I *.25
COMPOUND A,Z=212, 84 PARTICLE A,Z= 5, 2
.40
.30
.20
.10
.0
-.10
DEF2
-.10
.0
.10
.20
.30
.40
DEF1

Fig. 2b

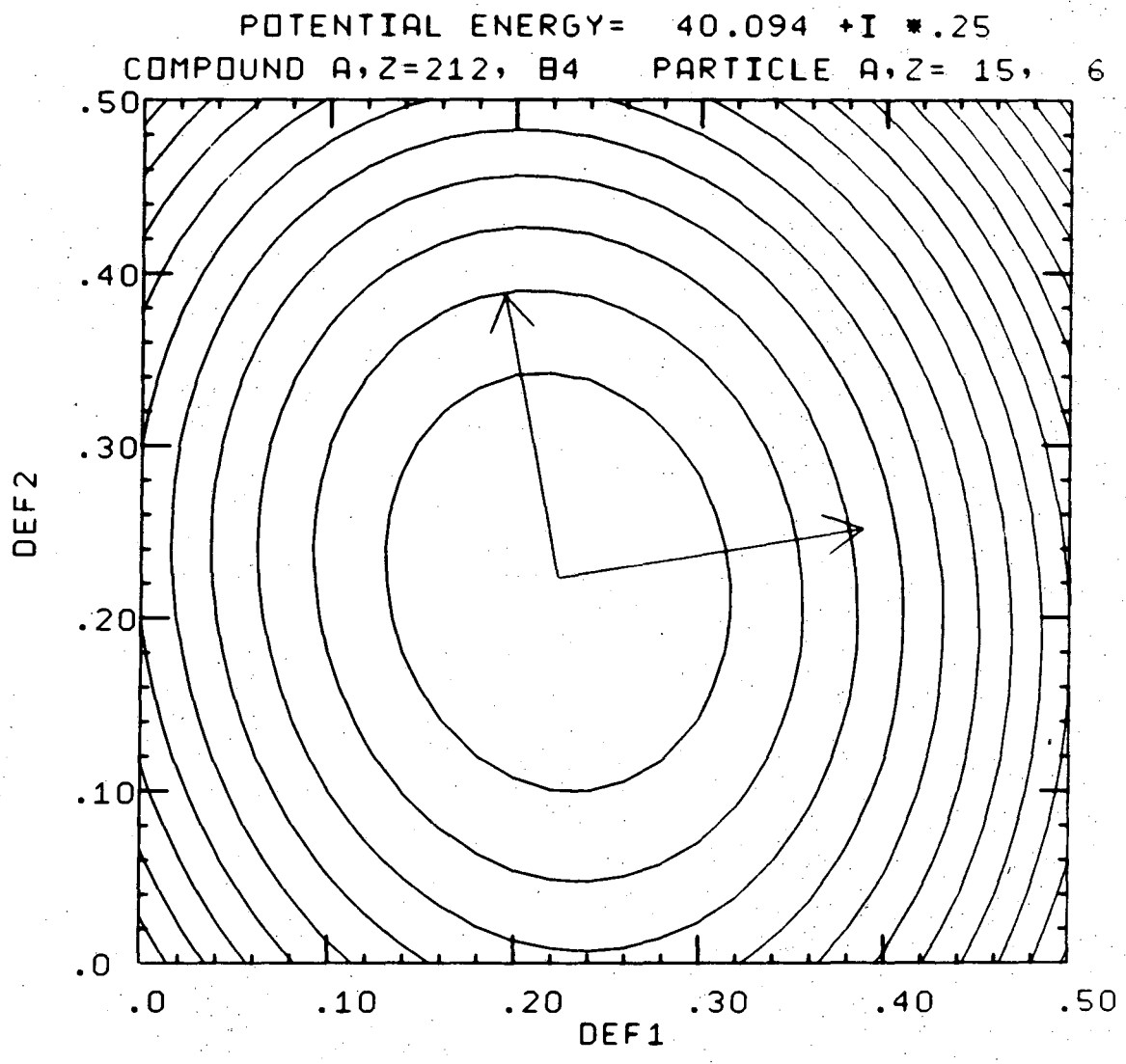
POTENTIAL ENERGY= 40.094 +I *.25
COMPOUND A,Z=212, 84 PARTICLE A,Z= 15, 6
.50
.40
.30
.20
.10
.0
DEF2
.0
.10
.20
.30
.40
.50
DEF1

Fig. 2c

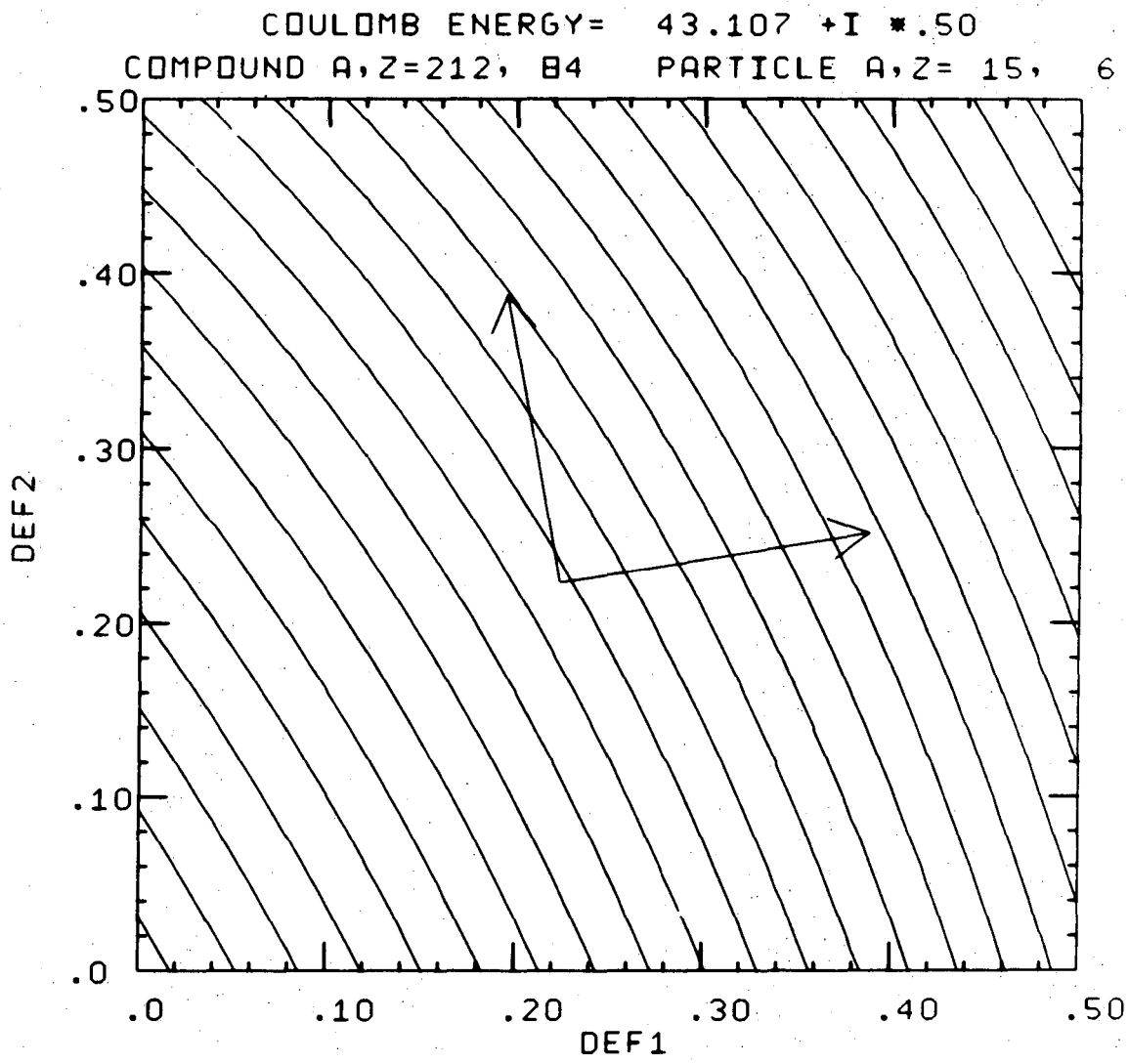
COULOMB ENERGY= 43.107 +I *.50
COMPOUND A,Z=212, 84 PARTICLE A,Z= 15, 6
.50
.40
.30
.20
.10
.0
DEF2
.0
.10
.20
.30
.40
.50
DEF1

Fig. 2d

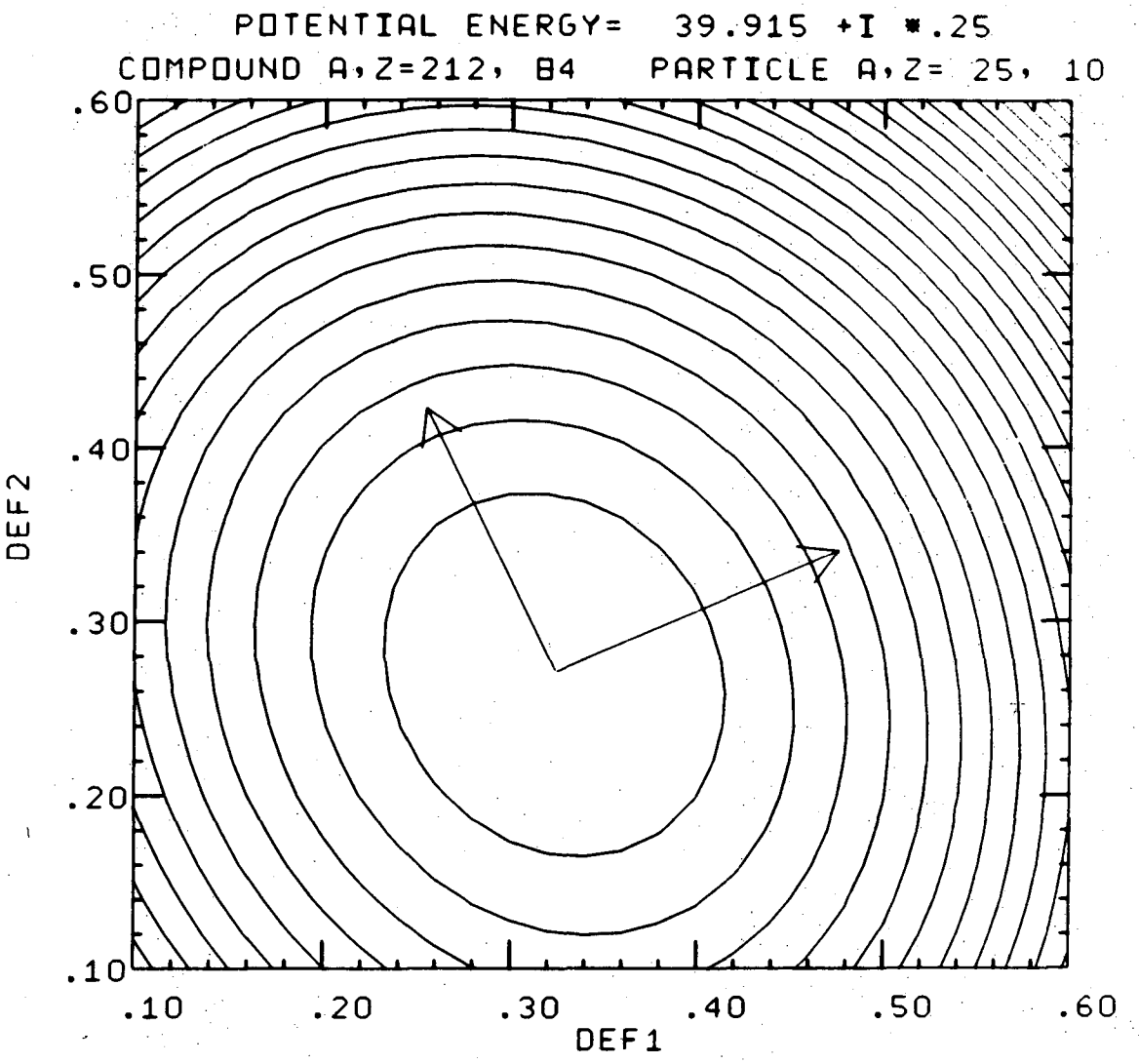
POTENTIAL ENERGY= 39.915 +I *.25
COMPOUND A,Z=212, 84 PARTICLE A,Z= 25, 10
.60
.50
.40
.30
.20
.10
DEF2
.10
.20
.30
.40
.50
.60
DEF1

Fig. 2e

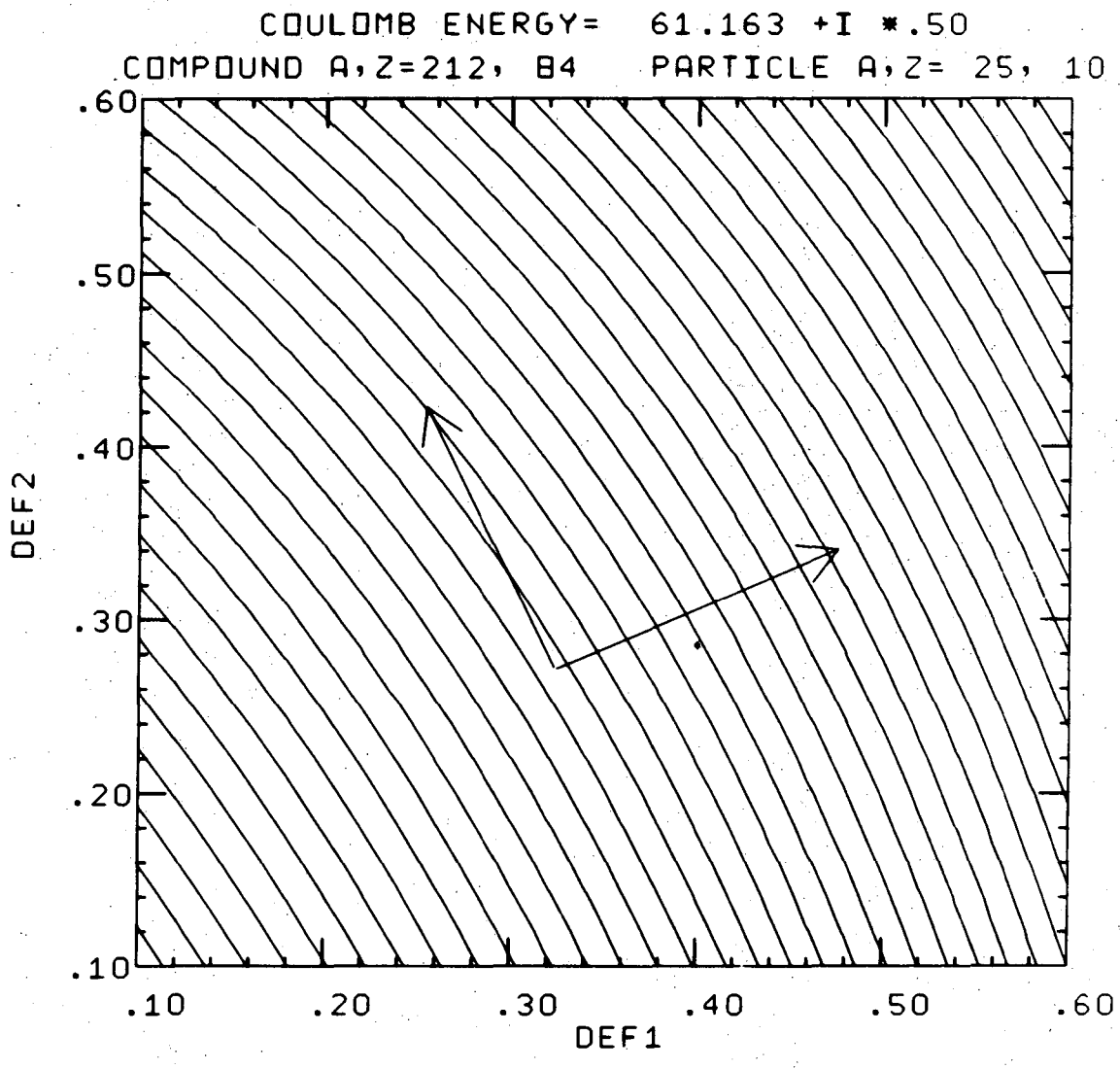
COULOMB ENERGY= 61.163 +I *.50
COMPOUND A,Z=212, 84 PARTICLE A,Z= 25, 10
.60
.50
.40
.30
.20
.10
DEF2
.10
.20
.30
.40
.50
.60
DEF1

Fig. 2f

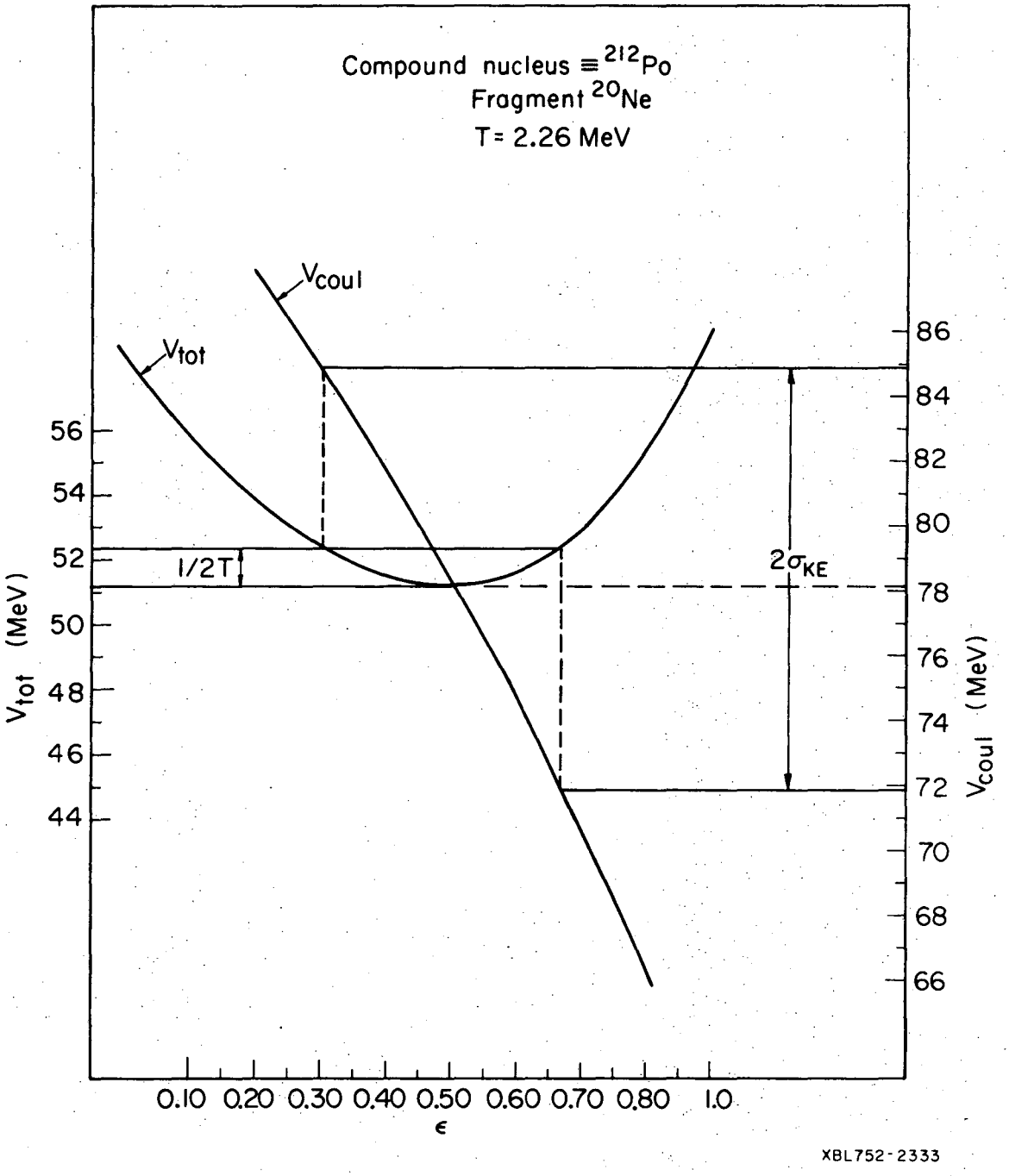
Compound nucleus ≡ ^{212}Po
Fragment ^{20}Ne
T= 2.26 MeV
V_{coul}
V_{tot}
1/2T
$2\sigma_{KE}$
V_{tot} (MeV)
V_{coul} (MeV)
56
54
52
50
48
46
44
86
84
82
80
78
76
74
72
70
68
66
0.10 0.20 0.30 0.40 0.50 0.60 0.70 0.80 1.0
ϵ
XBL752-2333

Fig. 3

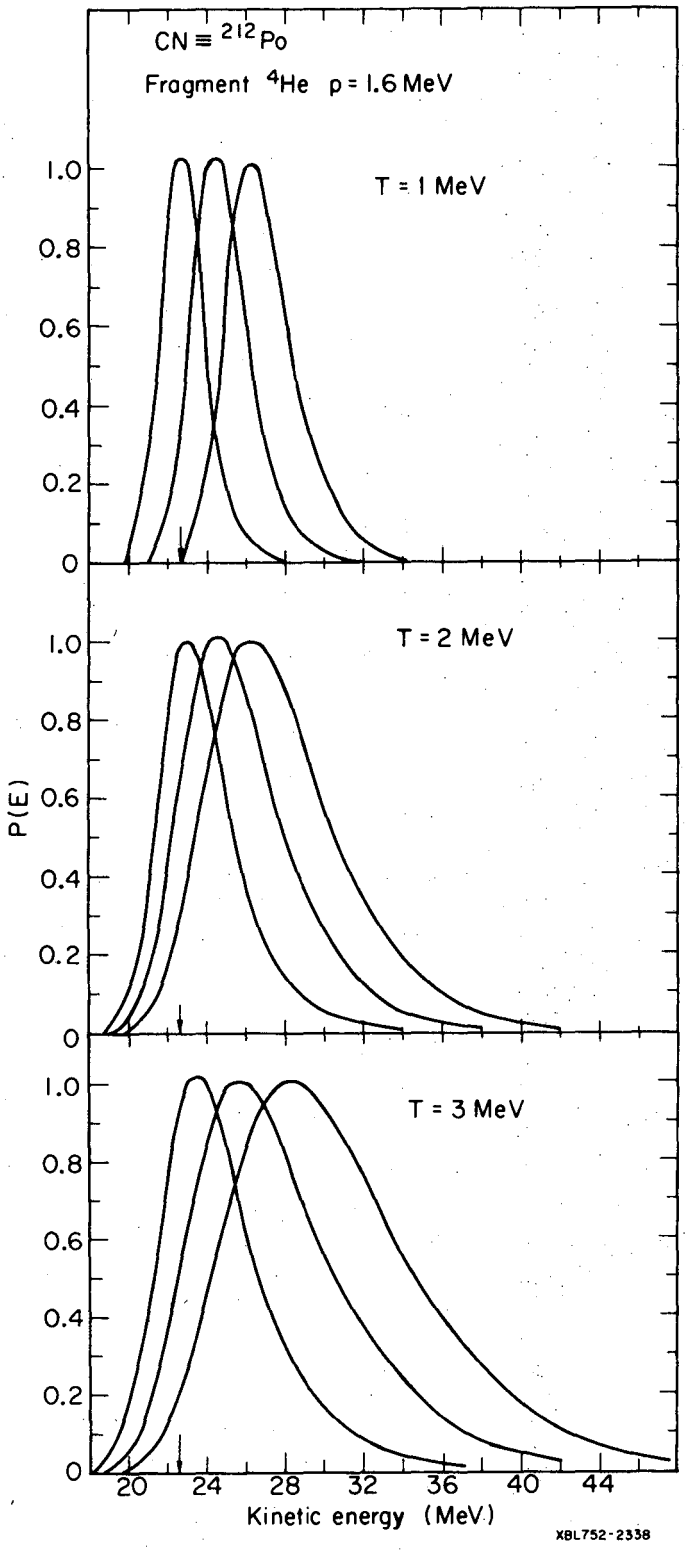
CN ≡ 212Po
Fragment 4He p = 1.6 MeV
T = 1 MeV
T = 2 MeV
T = 3 MeV
P(E)
1.0
0.8
0.6
0.4
0.2
0
20
24
28
32
36
40
44
Kinetic energy (MeV)
XBL752-2338

Fig. 4a

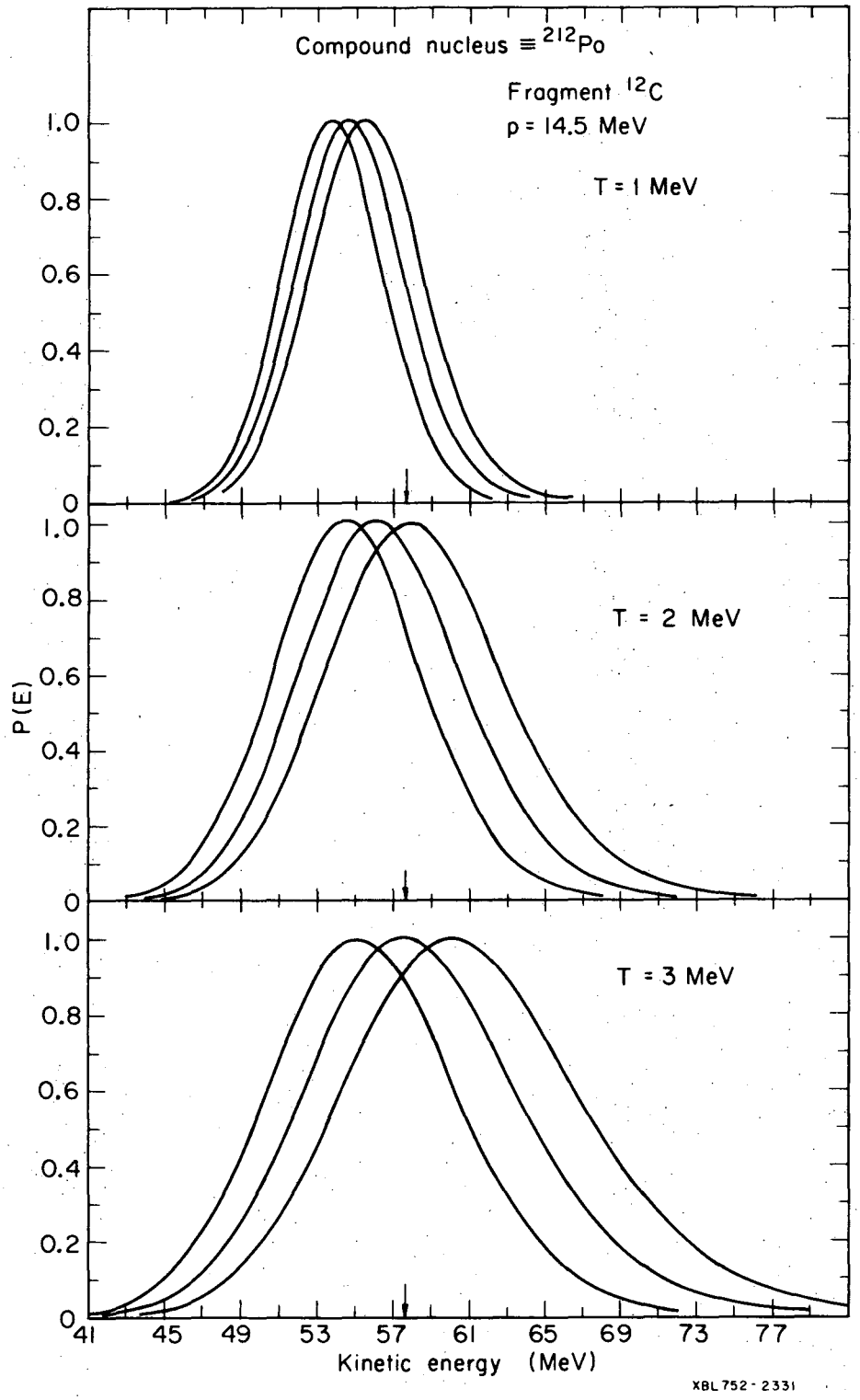
Compound nucleus ≡ ^{212}Po
Fragment ^{12}C
p = 14.5 MeV
T = 1 MeV
T = 2 MeV
T = 3 MeV
P(E)
0
0.2
0.4
0.6
0.8
1.0
41
45
49
53
57
61
65
69
73
77
Kinetic energy (MeV)
XBL752-2331

Fig. 4b

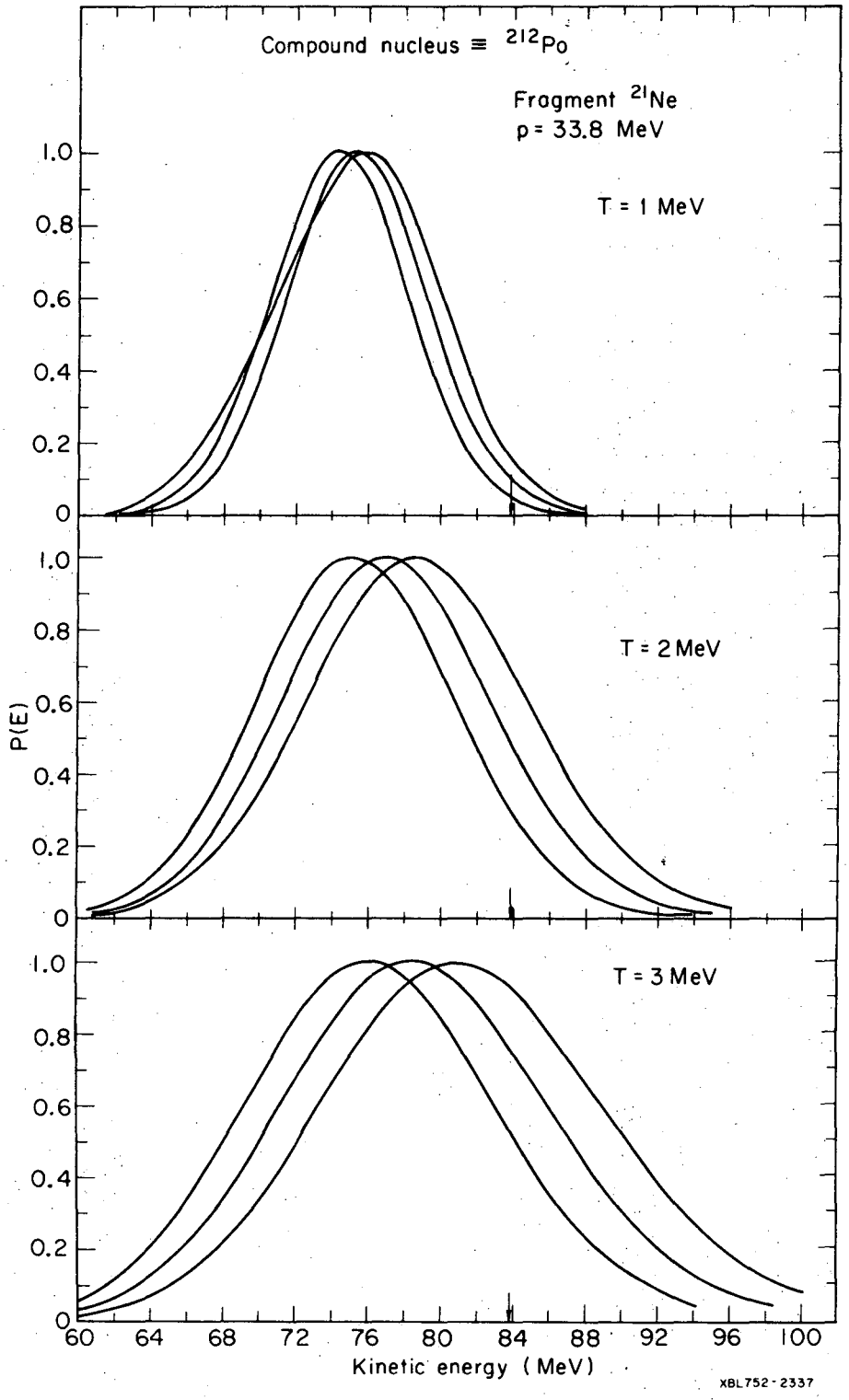
Compound nucleus ≡ ^{212}Po
Fragment ^{21}Ne
p = 33.8 MeV
T = 1 MeV
T = 2 MeV
T = 3 MeV
P(E)
1.0
0.8
0.6
0.4
0.2
0
60
64
68
72
76
80
84
88
92
96
100
Kinetic energy (MeV)
XBL752-2337

Fig. 4c

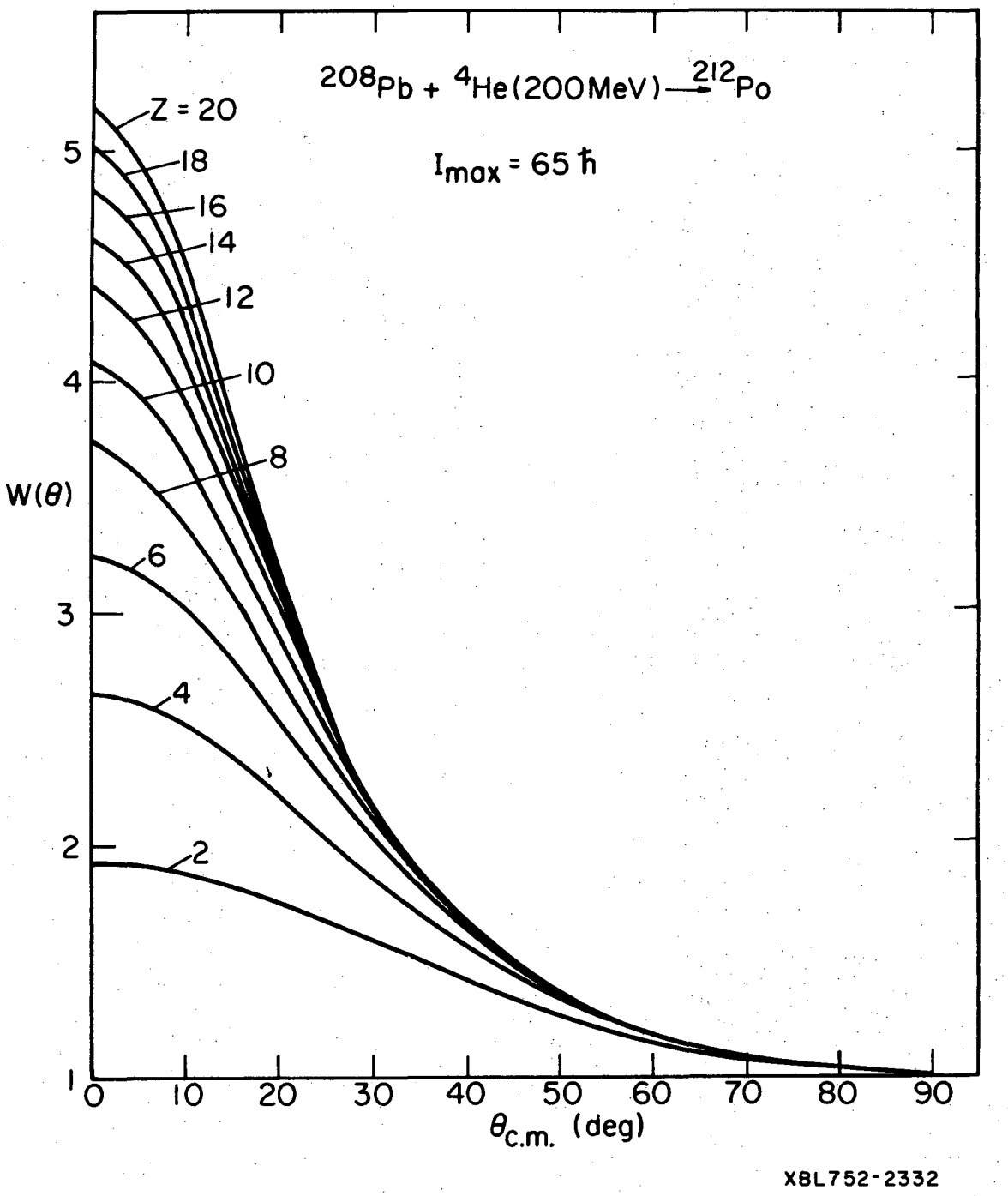
$^{208}Pb + {}^{4}He(200MeV) \rightarrow {}^{212}Po$
$I_{max} = 65\,\hbar$
Z = 20
18
16
14
12
10
8
6
4
2
W(θ)
θc.m. (deg)
0
10
20
30
40
50
60
70
80
90
1
2
3
4
5
XBL752-2332

Fig. 5

TECHNICAL INFORMATION DIVISION
LAWRENCE BERKELEY LABORATORY
UNIVERSITY OF CALIFORNIA
BERKELEY, CALIFORNIA 94720